International Journal of Minerals, Metallurgy and Materials
Volume 22, Number 10, October 2015, Page 1005
DOI: 10.1007/s12613-015-1162-3

Ultra-fine grinding and mechanical activation of mine waste rock using a high-speed stirred mill for mineral carbonation

Jia-jie Li and Michael Hitch

Norman B. Keevil Institute of Mining Engineering, University of British Columbia, Vancouver V6T 1Z4, Canada
(Received: 14 February 2015; revised: 21 April 2015; accepted: 22 April 2015)

Abstract: CO_2 sequestration by mineral carbonation can permanently store CO_2 and mitigate climate change. However, the cost and reaction rate of mineral carbonation must be balanced to be viable for industrial applications. In this study, it was attempted to reduce the carbonation costs by using mine waste rock as a feed stock and to enhance the reaction rate using wet mechanical activation as a pre-treatment method. Slurry rheological properties, particle size distribution, specific surface area, crystallinity, and CO_2 sequestration reaction efficiency of the initial and mechanically activated mine waste rock and olivine were characterized. The results show that serpentine acts as a catalyst, increasing the slurry yield stress, assisting new surface formation, and hindering the size reduction and structure amorphization. Mechanically activated mine waste rock exhibits a higher carbonation conversion than olivine with equal specific milling energy input. The use of a high-speed stirred mill may render the mineral carbonation suitable for mining industrial practice.

Keywords: mineral carbonation; mine wastes; mechanical activation; grinding

1. Introduction

Carbon capture and sequestration (CCS) is widely recognized as the quickest and most efficient way to solve the problem of climate change caused by CO_2 emissions [1]. CO_2 sequestration by mineral carbonation is the only known process that can permanently store anthropogenic CO_2 [2]. Mineral carbonation mimics the natural weathering of Ca/Mg silicates and involves three steps: CO_2 dissolution into rainwater, dissolution of Ca/Mg silicates, and precipitation of Ca/Mg carbonates and silica. Olivine and serpentine are the most abundant minerals suitable for mineral carbonation. The mineral carbonation reaction on both minerals is simply described in Eqs. (1) and (2). These thermodynamically favorable processes are extremely slow, naturally occurring over millennia.

$$Mg_2SiO_4 + 2CO_2 \rightarrow 2MgCO_3 + SiO_2 \quad (1)$$

$$Mg_3Si_2O_5(OH)_4 + 3CO_2 \rightarrow 3MgCO_3 + 2SiO_2 + 2H_2O \quad (2)$$

CO_2 sequestration by mineral carbonation was first proposed in 1990; since then, the researchers have sought ways to accelerate the process with less energy consumption [2]. Despite these efforts, the process has yet to be economically developed. The use of inexpensive feedstock, the development of a less energy-intensive pre-activation method, and the elimination of the use of chemicals could reduce the costs of mineral carbonation [3].

Mine waste rocks (especially tailings) from ultramafic-hosted ore deposits, including nickel, copper, chromium, and platinum-group element deposits, are favored mineral carbonation processes [4]. Ultramafic-hosted mines could benefit from the mineral carbonation of their waste material, with the final products adding value through secondary revenue [5]. The economical mineral-free tailings are fine-sized grains that are rich in magnesium silicates. Using mine waste rock as a potential substrate for mineral carbonation reduces the need for a primary energy-consumptive grinding stage [6]. As the base metal resources become increasingly fine-grained, beneficiation and refractory processes are needed to grind them to increasingly finer sizes, even to the ultra-fine range (median particle size, $d_{50} < 10$ μm) [7]. In this case, the operational energy consumption of mechanical activation as a pre-treatment method for mineral

Corresponding author: Jia-jie Li E-mail: jiajie.li@alumni.ubc.ca

carbonation could be reduced to a more practical level when mechanical activation is integrated as a part of the total milling process [8].

Mechanical activation uses mechanical energy to change the physical, chemical, and structural behaviors of materials, thereby enhancing the downstream reactions [9]. Compared with the conventional comminution, the effects of mechanical activation are not limited to a decrease in the particles size and an increase in the surface area. Mechanical activation also stores excess energy as long-lived defects through the introduction of imperfections into the crystal lattice, which is essential for the materials to overcome the activation energy in downstream reactions [10]. The necessary level of mechanical activation can be achieved by prolonged grinding in a high-intensity mill, such as a planetary mill, attrition mill, or vibratory mill [9].

Mechanical activation has the ecologically clean attributes (i.e., no chemicals added) and offers a high activation extent that is similar to that of calcination, which makes this process preferable to thermal and chemical activation [2]. The mechanical activation of olivine [8,11–14] and serpentine [3,15–16] has been studied in detail. These studies have all demonstrated an acceleration of the carbonation process or other downstream acid leaching processes. Because of the difference in physical features, chemical composition, and crystal structure of olivine and serpentine, the mechanisms for mechanical activation on each mineral also differ. For example, the serpentine easily becomes amorphous through dry grinding. This transformation has been observed through the partial disappearance of X-ray diffraction (XRD) peaks of serpentine after a 120-min dry grinding, whereas the XRD peaks of forsterite remain even after 240 min of grinding [15]. Mine waste rocks are always mixtures containing both primary ultramafic minerals (olivine) and weathered minerals (serpentine). Because both minerals are favorable for mineral carbonation, studying the mechanical activation of such mixtures is important for saving energy during the separation process.

Previous studies have primarily focused on the individual minerals, and the interactions between both minerals during mechanical activation and downstream carbonation have yet to be investigated. Thus far, batch-mode grinding has been adopted in most cases of mechanical activation. Continuous grinding has the potential to enhance the energy efficiency and enlarge the production quantity [11], which could push the mechanical activation into widespread application.

In this study, the changes in slurry rheological properties, particle size, surface area, and crystallinity of mine waste rock and pure olivine were investigated during fine grinding and mechanical treatment under wet conditions. An IsaMill operated in continues mode was chosen for the purpose of mechanical activation because this type of stirred-ball mill has been successfully used for ultrafine grinding. Because of its quick response to CO_2 sequestration, a direct aqueous mineral carbonation process was used to test the extent of mechanical activation. The aim was to study the interaction between serpentine and olivine during the process of mechanical activation under wet conditions for mineral carbonation.

2. Materials and experiments

2.1. Materials

The mine waste rock or whole ore (06-110) used in this study was provided by Hard Creek Nickel from a 06-110 drill core from their Turnagain deposit in northern British Columbia, Canada. The olivine foundry sand (OL-NW) was provided by OCL Industrial Materials, Ltd., and originated from Norway. The elemental composition of the as-received materials is given in Table 1. X-ray powder diffraction analysis indicated a mineral composition of 64.7wt% forsterite, 29.6wt% lizardite, 4.2wt% magnetite, 0.3wt% quartz, and 2.5wt% brucite in 06-110. OL-NW was determined to contain 95.7wt% forsterite, 1.3wt% enstatite, 0.5wt% lizardite, 0.3wt% talc, 1.5wt% magnetite, 0.3wt% quartz, and 0.4wt% brucite. Forsterite is the magnesium end member of the olivine group, and lizardite is a polymorph of the serpentine-group of minerals. OL-NW is similar to the mineral used in various mechanical activation works in Norway [8,13]. Both the received materials were ground by a laboratory bond ball mill and screened using 140 mesh Tyler sieve (106 μm). The undersized materials were used as the feed for the IsaMill. Because of the low grade of nickel in the Turnagain project, the composition of mine waste rock and whole ore should be similar, allowing 06-110 to be considered as mine waste rock.

2.2. Grinding tests

The laboratory grinding tests were conducted using a 4-L IsaMill (Netzsch, Germany). The IsaMill is a horizontal stirred ball mill with an effective volume of 2.48 L. The agitator shaft for the mill has seven polyurethylene discs, each with a diameter of 0.106 m. 80% of the mill chamber volume is filled with Keramax MT1 ceramic beads with a diameter of 2 mm. Pulp, with a solids content of 30% by weight, was prepared by mixing 5 kg of samples and 11.7 kg of water. For each test, the slurry was fed into the mill, ground, collected, sampled, and then re-fed into the mill. This cycle was re-

peated up to nine times, during which the chamber temperature reached 40°C. The flow rate was controlled at 2–3 L/min. The agitator speed was maintained at 1500 r/min for the tests. The applied parameters and procedures were the general ones provided by Xstrata for the development of the signature plot, which was used to design a full-scale IsaMill [17]. The sampled slurry from each cycle was dried in an oven at 100°C overnight and subsequently deagglomerated. Samples from the feed, pass 1, pass 4, and pass 9 were selected for the carbonation and characterization tests.

Table 1. X-ray fluorescence (XRF) main and trace analysis results for the olivine samples (OL-NW) and mine waste (06-110)

Component	OL-NW / wt%	06-110 / wt%	Component	OL-NW / ppm	06-110 / ppm
SiO_2	40.700	38.700	Cu	12	3
Al_2O_3	0.150	0.150	Zn	18	43
Fe_2O_3	8.390	10.390	Ni	2986	2263
CaO	0.090	0.300	Co	120	124
MgO	50.940	45.510	Mn	852	1267
MnO	0.120	0.160	Sr	n/d	2
TiO_2	0.020	0.030	V	n/d	25
Cr_2O_3	0.677	0.671	La	n/d	2
LOI	n/d	4.090	Sn	n/d	2
TOT/C	n/d	0.050	Nb	n/d	n/d
TOT/S	0.060	0.030	Sc	2	5

Note: n/d stands for the value below the detection limit, LOI the loss on ignition which presents the volatile content, such as water, TOT/C the total C tested by Leco method, and TOT/S the total S tested by Leco method.

2.3. Carbonation tests

For the carbonation tests, 7.5 g of dried samples were mixed with 50 mL of background solutions containing 1 mol/L NaCl and 0.64 mol/L $NaHCO_3$; the resulting mixtures were transferred to a 100 mL autoclave (Parr Instruments, Moline, IL, USA). The background solution helped to achieve the optimum extent of carbonation by increasing the concentration of HCO_3^- in the aqueous solution and maintaining a constant pH value between 7 and 8 [12]. The slurry samples were carbonated at 185°C and 6 MPa CO_2, with a stirring speed of 1500 r/min over a period of 1 h. The carbonation conditions were chosen according to the optimum conditions for the direct aqueous mineral carbonation of olivine [12], the only difference being that the CO_2 pressure in this work was approximately two-fifths of the optimum pressure (15 MPa) because of the limitations of experimental setup. Also, it was expected that the mechanical activation could enable the use of milder carbonation conditions, resulting in lower carbonation expenses.

2.4. Materials characterization

The elemental compositions of the as-received materials were analyzed by Acme Analytical Laboratories, Ltd. (Vancouver) using X-ray fluorescence (XRF) spectroscopy and inductively coupled plasma mass spectrometry (ICP-MS) techniques. The rheological properties of settling suspensions were measured using an elongated concentric cylinder fixture developed by Klein *et al.* [18]. The particle size distribution (PSD) was measured with a laser diffraction particle size analyzer (Mastersizer 2000, Malvern, U.K.). The specific surface areas and porosities were measured by a nitrogen gas adsorption/desorption instrument (Autosorb-1MP, Quantachrome) at −198°C. The particle shape and morphology were observed using a Helios NanoLab 650 focused ion beam scanning electron microscope (FEI, Eindhoven, The Netherlands) equipped with a secondary electron detector; the microscope was operated at 50 pA and 1 kV. X-ray diffraction data for microstructure analysis and quantitative analysis were collected using a Bruker D8 Focus Bragg–Brentano diffractometer (Bruker AXS GmbH, Germany) equipped with a Co K_α radiation source; the samples were scanned at a step size of 0.03° over the 2θ range from 3° to 80°. X-ray powder diffraction data were refined with the Rietveld program Topas 4.2 to determine the amounts of carbon minerals present before and after mineral carbonation.

3. Results and discussion

The energy consumption, throughput, and size reduction for fine and ultra-fine grinding processes are complicated,

involving a large number of process parameters. As one example, for a stirred ball mill, Molls and Hornle have identified 44 such parameters [19]. The most important of these parameters are the process state and mill configuration variables. Process state variables include PSD, shape of feed, solid density, slurry density, slurry flow rate, and slurry rheology. Mill configuration variables include impellor design, mill speed, media size, media load, and media density [19]. Empirical methods, such as the bond method and population balance model, have demonstrated that power consumption vs. size reduction in coarse grinding ranges is no longer suitable for application to ultra-fine grinding. Analysis of the relationship between energy consumption and ultrafine grinding will aid in the evaluation and optimization of all of the primary operating parameters of a mill in a well-planned and executed laboratory or pilot test.

3.1. Energy consumption

The net specific energy consumption (W_N) is usually used to compare the energy efficiency for modifying the properties of materials under various milling conditions [8]. In a stirred mill, energy is transmitted from the agitator to the grinding media and the slurry, and is subsequently transferred to the particles through impact, compression, and abrasion loading. W_N represents the energy transferred to the charge and can be calculated through Eqs. (3)–(5). The residence time (t_M) in the IsaMill is calculated according to Eq. (6).

$$P_N = P_0 - P_{NL} \tag{3}$$

$$W_N = \frac{P_N}{M} \tag{4}$$

$$M = Q \cdot C \cdot \rho \tag{5}$$

$$t_M = \frac{V}{Q} \tag{6}$$

where P_0 is the operational power (kW), P_{NL} the average power draw when running the mill empty with no water or media (kW), P_0 and P_{NL} can be read from the agitator panel, M the mass of sample milled per hour (t/h), Q the flow rate of sample feed in the mill chamber (m^3/h), C the solid content by weight (%), ρ the slurry density (t/m^3), and V the net mill volume (2.4 L). Table 2 summarizes the power-related parameters of each milling cycle. The flow rate is constant in OL-NW and in the initial cycles of 06-110. After cycle 8, an observed decrease in the flow rate of 06-110 results in a longer residence time in subsequent cycles.

Table 2. Power parameters during grinding of 06-110 and OL-NW in an IsaMill

Pass No.	06-110						OL-NW				
	P_{NL} / kW	P_0 / kW	P_N / kW	W_N / (kWh·t^{-1})	Cum. W_N / (kWh·t^{-1})	t_M / s	P_0 / kW	P_N / kW	W_N / (kWh·t^{-1})	Cum. W_N / (kWh·t^{-1})	t_M / s
1	0.80	3.6	2.80	45.4	45.4	50	4.8	4.00	66.9	66.9	52
2	0.80	3.5	2.70	45.3	90.7	102	4.8	4.00	66.2	133.1	103
3	0.80	3.6	2.80	47.1	137.8	154	4.2	3.40	53.6	186.7	151
4	0.80	2.9	2.10	35.0	172.9	205	3.8	3.00	49.6	236.3	202
5	0.80	2.8	2.00	32.0	204.9	254	3.6	2.80	44.5	280.8	251
6	0.80	2.7	1.90	30.9	235.8	304	3.5	2.70	44.2	325.0	302
7	0.80	2.7	1.90	31.1	266.9	354	3.3	2.50	39.7	364.7	350
8	0.80	2.5	1.70	35.6	302.5	418	3.3	2.50	41.9	406.6	402
9	0.80	2.5	1.70	35.5	338.0	482	3.3	2.50	40.9	447.5	453

Note: Cum. W_N represents to the cumulative net specific energy consumption which can be used as the specific energy input at corresponding t_M.

3.2. Slurry rheological properties

The rheological data of grinding slurries were modeled using the Bingham flow curve equation [20], as shown in Eq. (7).

$$\tau = \tau_y + \eta\gamma \tag{7}$$

where τ is the shear stress (Pa), τ_y the Bingham yield stress (Pa), η the Bingham viscosity (Pa·s), and γ the shear rate (s^{-1}).

Fig. 1 shows the change in yield stress of slurry during IsaMill grinding. With the energy input, the yield stress increases because of the generation of fine particles, which is in agreement with the observed rheological properties of stirred mill slurries [21]. The increase rate of yield stress during grinding of 06-110 is much higher than that during grinding of OL-NW. This difference is a consequence of the presence of anisotropic and non-spherical-shaped serpentine minerals in 06-110. The serpentine suspension, especially chrysotile with fibrous shape, exhibits the high yield stress and viscosity [22]. High viscosity and yield stress reduce the

grinding efficiency and adversely affect comminution [21]. The increase in the yield stress of slurry can explain the significant decrease in the flow rate of 06-110 at pass 8.

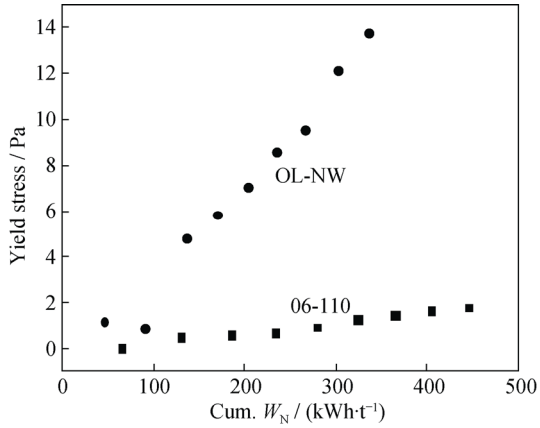

Fig. 1. Yield stress of slurries with specific energy input.

3.3. Mechanical activation effects

Mechanical activation effects are usually observed to occur in response to changes in particle size, surface area, and degree of amorphization. All these attributes of the materials are characterized for the sake of comparison with previously published results. Table 3 lists the mean particle size (P_{50}), the specific surface area (S_{BET}), the average degree of amorphization on forsterite (A_{Fo}), and the degree of amorphization on lizardite (100) phase ($A_{Li(100)}$) of the feed materials and the products from passes 1, 4, and 9.

(1) Particle size

The specific milling energy input vs. the 80% passing size (P_{80}) is drawn in a log-log plot, which is commonly used for designing a full-scale stirred mill from lab-sized tests [17]. Fig. 2 shows the signature plot of an IsaMill for 06-110 and OL-NW. The decrease in P_{80} follows an exponential function with the specific energy input for both materials, as shown in Eqs. (8)–(9). The continuous decrease in P_{80} with this specific milling energy input is consistent with the results reported in a previous study of the mechanical activation of olivine under wet conditions [8].

$$\text{OL-NW:}\quad W_N = 1332 P_{80}^{-0.93} \tag{8}$$

$$\text{06-110:}\quad W_N = 1002 P_{80}^{-1.028} \tag{9}$$

Table 3. Physical and structural parameters of the selected samples during milling in an IsaMill

Pass No.	06-110				OL-NW			
	P_{50} / μm	S_{BET} / (m^2·g^{-1})	$A_{Li(100)}$ / %	A_{Fo} / %	P_{50} / μm	S_{BET} / (m^2·g^{-1})	$A_{Li(100)}$ / %	A_{Fo} / %
Feed	35.4	3.1	0	0	74.1	0.7	0	0
1	7.2	7.2	–35	1.4	10.8	2.1	26.6	20.8
4	2.6	12.6	–32	0	3.4	8.6	25.7	24.0
9	1.6	17.8	–2	8.7	1.9	15.5	50.0	34.5

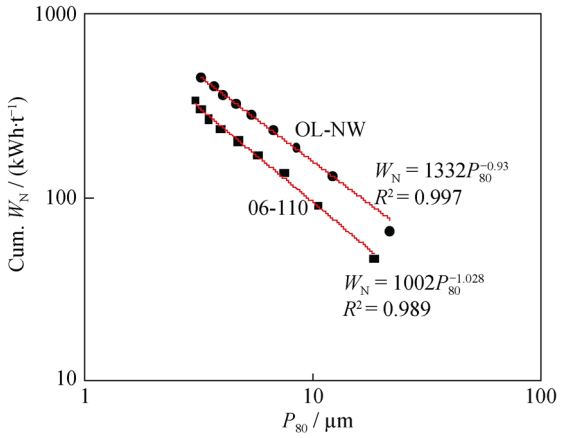

Fig. 2. Signature plot for the IsaMill.

The particle size of 06-110 is smaller than that of OL-NW in all grinding cycles. The mean particle sizes (P_{50}) recorded in Table 3 show the same trend. Because the feed particle size of 06-110 is smaller than that of OL-NW, merely comparing the actual particle size is insufficient for explaining the changes. Specific breakage energy, which describes the amount of energy required to reduce a particle size by one micron [23], was used to analyze the mill breakage efficiency. Under the assumption that the P_{80} was reduced from 100 to 2 μm, the average specific breakage energies calculated from Eqs. (8) and (9) were 6.94 and 4.92 kWh·t^{-1}·μm^{-1}, respectively. These results indicated that 06-110 was easier to break down to a fine size.

As shown in Fig. 2, the actual specific breakage energy is slightly higher than the calculated value in mechanically activated 06-110 when the particle size is less than 3 μm. However, this is not the case in the mechanically activated OL-NW, possibly because of the increasing yield stress in the slurry during grinding of 06-110, as discussed in section 3.2. This phenomenon can also be explained by the material properties related to the grinding limit. The grinding limit is an important parameter in a fine grinding approach, wherein the particle size no longer changes [23]. Deep stages of mechanical activation can be substituted if the grinding limit

reaches the brittle-plastic transition [24]. Soft materials break quicker and reach their grinding limit faster than harder materials [23]. The Mohs hardness of serpentine is 2.5–4 and that of olivine is 6.5–7 [25]. The high specific breakage energy in 06-110 indicates that the lizardite may reach its grinding limit at the seventh pass. This observation agrees with the results of breakage mechanism studies on silica and galena mixtures ground in an IsaMill [23]. Because the weight ratio of forsterite and lizardite in the mixture is 2.3:1, the forsterite breakage mechanism effect is dominant in 06-110. Forsterite does not appear to reach the grinding limit because the actual and calculated specific breakage energies agree with each other until pass 9 in the case of OL-NW.

(2) Specific surface area and morphology

The results in Table 3 show that the specific surface areas increase linearly with increasing energy input during IsaMill grinding. The same trend has been observed in other studies related to mechanical activation by wet grinding in attritors [8,13]. Fig. 3 shows the results of a comparison of our experimental data with that from the literature. The IsaMill exhibits greater efficiency in generating new surfaces compared to the attritor used by Baláž *et al.* [13] and the stirred mill used by Haug [8]; its efficiency is similar to that of the stirred media detritor (SMD), but less efficient than the attritor mill (AM) used by Summers *et al.* [14]. Because the energy consumption for AM is calculated using the Society for Mining, Metallurgy, and Exploration (SME) work index formula [14], the results may contain errors. The IsaMill exhibits greater efficiency than the conventional ball mill and other stirred mills with respect to size reduction in the fine range, and is consistent with previously reported results [19]. An energy input greater than 500 kWh/t is outside the scope of this work because it is only considered energy input levels relevant in industrial applications. The specific surface area of milled 06-110 is greater than that of OL-NW, irrespective of specific energy input, as shown in Fig. 3. This difference is mainly due to the finer particles in 06-110 compared to those in OL-NW.

Fig. 4 shows the scanning electron microscopy (SEM) micrographs of both products from pass 9, where some sharp particles approximately 1 μm in diameter are still present in both samples. The presence of these particles indicates that forsterite is highly resistant to milling. A similar result has been reported in a study on olivine morphology after wet milling in an attritor [14]. Both the OL-NW and 06-110 samples contain aggregates with nanoparticles. The nanoparticles in OL-NW are spherically shaped with smooth surfaces, as shown in Fig. 4(a), whereas those in 06-110 are noodle-shaped with rough surfaces in Fig. 4(b). The circular particles with a smooth surface (forsterite) indicate that the breakage mechanism is transgranular, whereas that of the counterpart (serpentine) is intergranular. These results agreed with those of Roufail [23], who observed that hard materials suffered the abrasion breakage across the grains, whereas soft materials endured the fracture breakage mostly along the grain boundaries at high agitating speeds in an IsaMill. The SEM micrograph in Fig. 4(a) confirms that the lizardite particles with rough surfaces contribute to the small particle size and large surface area in 06-110.

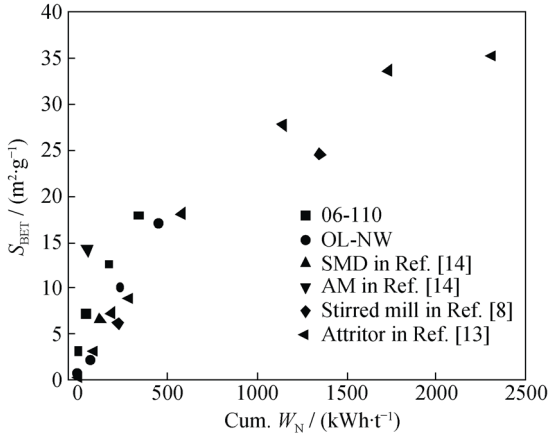

Fig. 3. Specific surface area as a function of specific energy input.

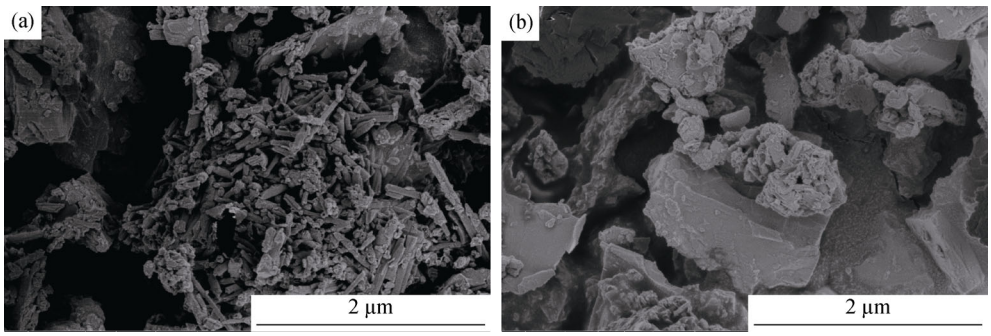

Fig. 4. SEM micrographs of the products from pass 9: (a) 06-110; (b) OL-NW.

(3) Degree of crystallinity and amorphization

XRD patterns are sensitive to the changes in the crystallinity of samples after mechanical activation. Fig. 5(b) shows the XRD peaks of forsterite in OL-NW become less intense and wider and the background level increases with increasing grinding energy input. A similar loss of crystallinity has also been detected in mechanically activated olivine in other stirred mills [8,13]. Contrary to expectations, 06-110 does not follow this pattern. Fig. 5(a) shows that the forsterite peaks of 06-110 are nearly unchanged and the lizardite (001) peak becomes even more intense than that in the feed in the first four cycles. Both minerals exhibit XRD peaks, even after being ground for 9 cycles, which indicates a large amount of crystallized forsterite and lizardite remained in the milled products. Eqs. (10)–(11) are used to calculate the crystallinity (C_{XRD}) and the degree of amorphization (A) of mechanically activated samples according to the XRD diffraction data [26]. The results are shown in Table 3.

$$C_{XRD} = \frac{B_0 I_x}{B_x I_0} \times 100\% \tag{10}$$

$$A = 1 - C_{XRD} \tag{11}$$

where I_0 and I_x are the integral intensity of diffraction peak for the non-activated mineral and the mechanically activated mineral, respectively, B_0 and B_x the background of diffraction peak for the non-activated mineral and the mechanically activated mineral, respectively. These equations assume that the non-activated mineral is 100% crystalline. C_{XRD} and A are bulk properties that include the effects of fine particle size, crystallite size, strain, and deformation of the crystal lattice.

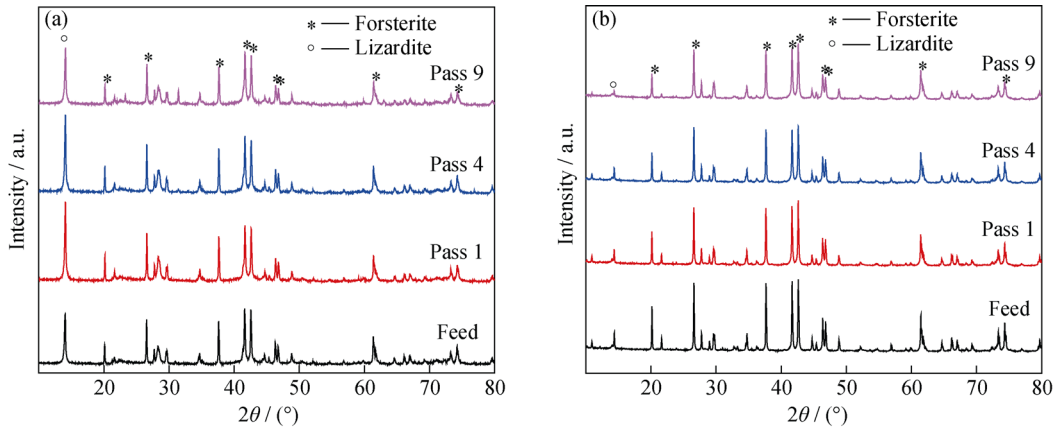

Fig. 5. XRD patterns of 06-110 (a) and OL-NW (b).

Table 3 lists the changes in the A values of forsterite (A_{Fo}) and lizardite ($A_{Li(001)}$) with specific energy input. A_{Fo} is the average value calculated on the basis of the (020), (021), (031), (131), (112), (221), (140), (222), and (260) forsterite diffraction peaks, which correspond to the peak positions (2θ) of approximately 20.1°, 26.6°, 37.7°, 41.7°, 42.6°, 46.4°, 46.9°, 61.5°, and 74.3°, respectively. $A_{Li(001)}$ is obtained from the lizardite (001) phase because mechanical activation is mainly affected along the c-axis of the lizardite structural unit [16]. The value of A_{Fo} initially increases quickly to 20.8% at pass 1 and then increases slowly to 34.5% at pass 9 in the case of mechanically activated OL-NW. However, the value of A_{Fo} remains nearly unchanged up to pass 4 and increases to 8.7% at pass 9 in the case of mechanically activated 06-110. The value of $A_{Li(001)}$ changes similarly to that of A_{Fo} in mechanically activated OL-NW because only a trace of lizardite (0.5%) is present in this material. In contrast, $A_{Li(001)}$ decreases to −35% in the first cycle in mechanically activated 06-110 and then increases with increasing specific energy input. The negative values of $A_{Li(001)}$ in the case of 06-110 indicate that the lizardite that appears in the ground products is more crystalline than that in the feed. Lizardite phase formation can be promoted in two ways: either through the conversion via the chemical reaction of forsterite with water or through the recrystallization from an amorphous phase. The latter approach is more likely in a lab setting because the XRD pattern of pure olivine does not show a distinct increase in the intensity of lizardite diffraction peaks. Lizardite has a planar disorder structure and is considered to be an amorphous phase in XRD analyses [6]. The conversion mechanism between the amorphous phase and the lizardite structure through wet milling is not the focus of this study.

In mineral carbonation, mechanical activation of lizardite in wet milling conditions did not promote the desired reaction and was therefore not recommended [3]. Studies related

to the activation of serpentine minerals were focused primarily on the removal of –OH bonds, either through dry milling or through a thermal treatment [27]. However, the influence of lizardite on the wet milling process should not be neglected. As seen in Table 3, when it is abundant in forsterite, lizardite appears to act as a dispersant to prevent or postpone the disorder in forsterite phases through wet milling.

The authors of several studies have used the diffraction peaks of forsterite (020) to calculate and represent C_{XRD} [8,13]. C_{XRD} was calculated in the same manner for purposes of comparison in this study. As shown in Fig. 6, the decrease in the value of C_{XRD} in the first cycle of IsaMill grinding is similar to that reported in the literature. Afterwards, the efficiency of C_{XRD} in the IsaMill is considerably less than that reported for other stirred mill tests. This difference may be attributable to the milling mode. The IsaMill is operated in continuous mode, whereas other stirred mill tests for mechanical activation are conducted in batch mode. Continuous-mode grinding can prevent overheating because the material passes through the grinding chamber quickly. At the same time, continuous-mode grinding reduces the chance of accumulating long-lived defects in samples and limits the deep imperfections in the sample.

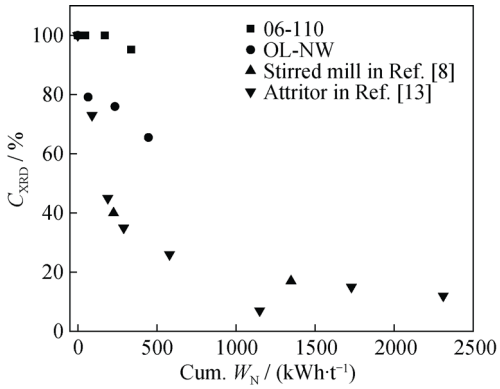

Fig. 6. Crystallinity as a function of specific energy input.

3.4. Effect of milling energy on mineral carbonation

Quantitative analysis of mine waste rock by Rietveld refinement was undertaken by Wilson [6] and was adopted in this study. In this method, lizardite was considered as an amorphous phase by fitting the structureless pattern to the planar disorder in lizardite. This method may overestimate the lizardite and underestimate other phases because of the surface roughness of all of the minerals. However, the phases with more than 5% abundance in mine waste rock can be estimated accurately with low absolute errors [6].

The extent of carbonation is expressed by the CO_2 sequestration reaction efficiency (R_X), which is the percentage stoichiometric conversion of Mg^{2+}, Ca^{2+}, and Fe^{2+} cations in the silicate feed to carbonate [12], as shown in Eq. (12).

$$R_X = \frac{X_{CO_2}}{\varepsilon_A (1 - X_{CO_2})} \tag{12}$$

where X_{CO_2} is the weight percent of CO_2 in the solid products and ε_A is the percent weight added if all available cations are converted into carbonates.

As shown in Fig. 7(a), R_X increases with the mechanical activation energy input. The R_X value of 06-110 is greater than that of OL-NW when the energy input is less than 350 kWh/t, indicating that the mechanical activation of mine waste rock that contains serpentine results in better carbonation efficiency than that achieved with pure olivine mineral. Similarly beneficial effects were observed in a study of the *in-situ* CO_2 mineral sequestration in partially serpentine peridotites [28]. Figs. 7(b)–(d) show that R_X increase with decreasing particle size, increasing surface area, and decreasing crystallinity. However, no evident difference in the trends between 06-110 and OL-NW is observed.

When carbonation potential is plotted with S_{BET}/C_{XRD} (as show in Fig. 7(e)), a linear correlation is observed in the initial phase of mechanical activation up to cycle 4, where C_{XRD} is the average crystallinity calculated according to nine selected forsterite peaks. The same results associated with the relation between the initial rate constant and the S_{BET}/C_{XRD} ratio has been reported in a study on the iron sulfate leaching of mechanically activated chalcopyrite [29]. The lower R_X per S_{BET}/C_{XRD} in 06-110 than in OL-NW is primarily due to the different lizardite contents. Materials after 9 cycles of grinding exhibit a large S_{BET}/C_{XRD} value; however, the carbonation potential is not as high as expected according to the extrapolation line obtained from previous cycles. The R_X reaches a maximum at 51%–53% during pass 9 for both materials. At this time, the rate of carbonation process is controlled by $MgCO_3$ precipitation instead of by magnesium silicate dissolution. In the case of a precipitation-controlled reaction, further mechanical activation is not necessary.

Fig. 8 shows the contents of forsterite, lizardite, and magnesite by mass in feed and carbonated products. Magnesite is the result of forsterite being carbonated under laboratory conditions. The content of lizardite remains the same. These results were in agreement with the results of the studies of direct aqueous mineral carbonation on mechanically activated serpentine ore, where the value of R_X did not exhibit a distinct increase even after being attrited for 1 h [3]. Therefore, a high content of forsterite in the raw material

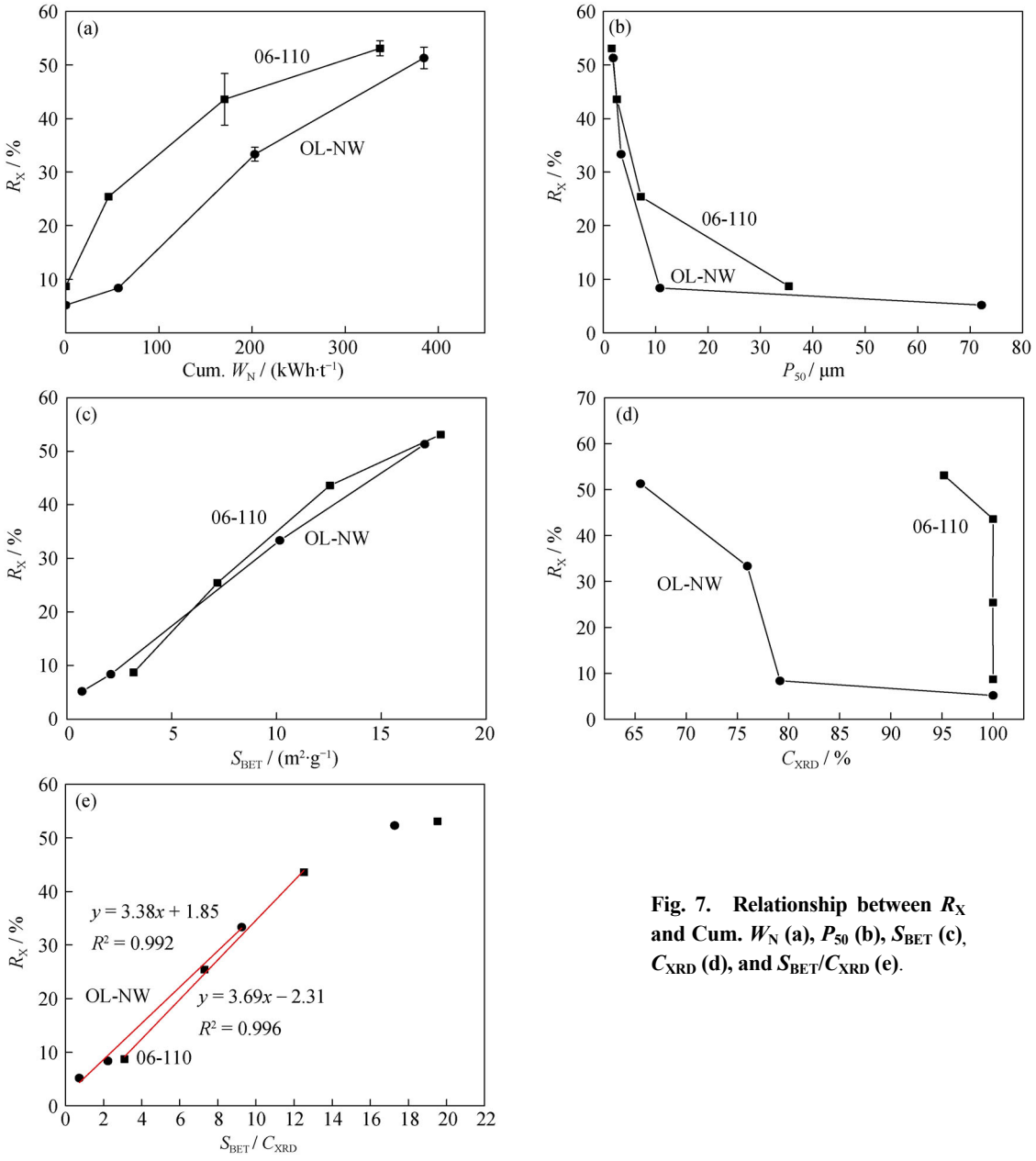

Fig. 7. Relationship between R_X and Cum. W_N (a), P_{50} (b), S_{BET} (c), C_{XRD} (d), and S_{BET}/C_{XRD} (e).

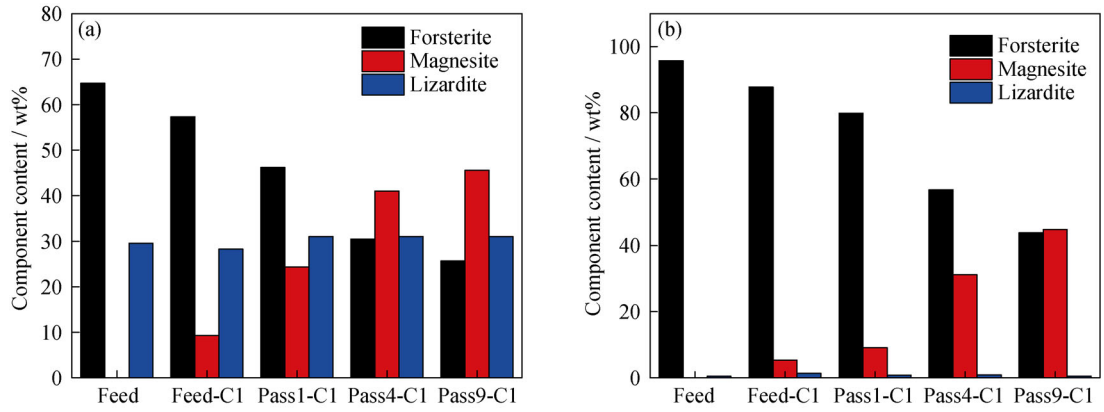

Fig. 8. Mineralogy changes in 06-11 (a) and OL-NW (b) after carbonation for 1 h, where Feed-C1, Pass1-C1, Pass4-C1, and Pass9-C1 represent the 1-hour carbonation product of feed and samples from pass 1, 4, and 9, respectively.

was required for choosing wet mechanical activation as a pretreatment method for mineral carbonation. Actually, under the high-carbonate alkalinity, olivine simultaneously produced magnesite and lizardite [30]. The most likely explanation for the higher R_X in mechanically activated 06-110 was that lizardite impurities acted as the catalyzers in the whole process. Lizardite promoted the surface area exposure for Mg^{2+} depletion in the solution. Simultaneously, lizardite precipitated with magnesite and maintained an equal quantity. Mechanically activated 06-110 was benefited from a large surface area under low specific energy input.

3.5. Comparison of the obtained results with reference data

Table 4 lists some reference results related to the direct aqueous carbonation of olivine and serpentine. The extent of carbonation for feed material in this work (R_X = 8.7% for 06-110 and R_X = 5.2% for OL-NW) is comparable to that reported in the literature for untreated olivine. The extent of carbonation of mechanically activated material after 8 min (R_X = 53.1% for 06-110 and R_X = 51.2% for OL-NW) is comparable to that reported in the literature for olivine (−38 μm) under carbonation at a CO_2 pressure four times greater than that used here. Thus, the extent of mechanical activation and the carbonation conditions can be balanced to achieve an economically optimal process. The carbonation conversion achieved this work is not as high as that reported by Summer *et al.* [14]; however, the relative increases in R_X are similar (84.3%/39.6% = 2.13 for grinding in AM in Ref. [14], and 53.1%/25.7% = 2.07 in our work). Greater carbonation conversion is achieved in the present investigation than in the investigation by Haug [8], which demonstrates the importance of the carrier solution for direct aqueous mineral carbonation. Methods to enhance the rate of magnesium carbonate precipitation are essential for the whole process because mechanical activation can only accelerate the process by enhancing the silicate dissolution rate.

Table 4. Reference data for direct carbonation of mechanically activated olivine and serpentine in batch experiments

Material	Mechanical activation	t_M / min	R_X / %	Carbonation condition	Ref.
Olivine	—	—	49.5	185°C, 25 MPa, 1 h, −38 μm, in 1 mol/L NaCl and 0.64 mol/L $NaHCO_3$	[31]
Olivine	—	—	39.6	185°C, 15 MPa, 1 h, −38 μm, in 1 mol/L NaCl and 0.64 mol/L $NaHCO_3$	[31]
Olivine	—	—	25.7	185°C, 6 MPa, 1 h, −38 μm, in 1 mol/L NaCl and 0.64 mol/L $NaHCO_3$	[31]
Olivine	—	—	5.1	185°C, 15 MPa, 1 h, −75 μm, in 1 mol/L NaCl and 0.64 mol/L $NaHCO_3$	[14]
Olivine	SMD	25	69.9	185°C, 15 MPa, 1 h, in 1 mol/L NaCl and 0.64 mol/L $NaHCO_3$	[14]
Olivine	AM	60	84.3	185°C, 15 MPa, 1 h, in 1 mol/L NaCl and 0.64 mol/L $NaHCO_3$	[14]
Olivine	Attritor	60	19.0	185°C, 11.5 MPa, 2 h, in water	[8]
Olivine	Attritor	60	87.0	185°C, 11.5 MPa, 18 h, in water	[8]
Serpentine	—	—	2.5	185°C, 15 MPa, 1 h, −38 μm, in 1 mol/L NaCl and 0.64 mol/L $NaHCO_3$	[31]
Pipe ore[a]	Attritor	15–60	7–9	155°C, 12.4 MPa, 1 h, in 1 mol/L NaCl and 0.64 mol/L $NaHCO_3$	[3]
OK ore[a]	Attritor	15–60	9–12	155°C, 12.4 MPa, 1 h, in 1 mol/L NaCl and 0.64 mol/L $NaHCO_3$	[3]

Note: [a] corresponds to the serpentine hosted nickel ore.

Compared to the batch-mode attritors, the IsaMill operated in continuous mode is equally efficient in producing new specific surfaces and demonstrates equal initial efficiency in reducing crystallinity. However, the overall efficiency of crystallinity reduction in the continuous mode is lower than that in the batch mode because the continuous mode permits energy relaxation during each cycle to prevent overheating. Because carbonation conversion is a linear function of S_{BET}/C_{XRD}, the mechanical activation by an attritor operated in continuous mode could promote amorphization through an increase in the residence time of the first cycle and through a decrease in the flow rate of slurry fed into the mill.

Further research and development of an overall economic analysis of a mineral processing plant that integrates the mineral carbonation process with mechanical activation as a pretreatment method will help to explain the feasibility of process in detail.

4. Conclusions

(1) When olivine and serpentine are ground concurrently, the yield stress of slurry increases dramatically and the breakage efficiency of mill decreases.

(2) The serpentine content in the mine waste rock facilitates an increase in the specific surface area, but prevents the crystallinity from being reduced during wet mechanical activation.

(3) Compared to pure olivine, mine waste rock stores more excessive energy during grinding in the form of S_{BET}/C_{XRD}, which leads to the greater carbonation conversion in a defined specific milling energy input.

(4) Forsterite is the main mineral being activated and carbonated, and lizardite catalyzes the whole process. The proposed process can be effectively applied when forsterite is the major phase in the mine waste rock.

(5) The attritor in continuous mode can activate olivine or mine waste rock within a short residence time and with a large production quantity; it is therefore viable for the industrial practice of mineral carbonation.

Acknowledgements

This work was financially supported by the State Scholarship Fund from the China Scholarship Council (No. 2008110820) and Carbon Management Canada. The authors would like to acknowledge Sally Finora, Jenny La, and Gethin Owen for analytical assistance and appreciate the advice of Mati Raudsepp regarding XRPD quantitative analyses and Ian Power regarding morphology analyses.

References

[1] Intergovernmental Panel on Climate Change (IPCC), *IPCC Fifth Assessment Report*: *Climate Change 2013 — The Physical Science Basis*, Eds. by T.F. Stocker, D. Qin, G.K. Plattner, *et al.*, Cambridge University Press, Cambridge, 2013, p. 1535.

[2] I.M. Power, A.L. Harrison, G.M. Dipple, S.A. Wilson, P.B. Kelemen, M. Hitch, and G. Southam, Carbon mineralization: From natural analogues to engineered systems, *Rev. Mineral. Geochem.*, 77(2013), No. 1, p. 305.

[3] E.R. Bobicki, Q.X. Liu, and Z.H. Xu, Mineral carbon storage in pre-treated ultramafic ores, *Miner. Eng*., 70(2015), p. 43.

[4] M. Hitch, S.M. Ballantyne, and S.R. Hindle, Revaluing mine waste rock for carbon capture and storage, *Int. J. Min. Reclam. Environ.*, 24(2010), No. 1, p. 64.

[5] M. Hitch and G.M. Dipple, Economic feasibility and sensitivity analysis of integrating industrial-scale mineral carbonation into mining operations, *Miner. Eng.*, 39(2012), p. 268.

[6] S.A. Wilson, *Mineral Traps for Greenhouse Gases in Mine Tailings: A Protocol for Verifying and Quantifying CO_2 Sequestration in Ultramafic Mines* [Dissertation], University of British Columbia, Vancouver, 2009, p. 315.

[7] B.A. Wills and T. Napier-Munn, *Will's Mineral Processing Technology*: *An Introduction to the Practical Aspects of Ore Treatment and Mineral Recovery* (*7th Ed.*), Butterworth-Heinemann, Oxford, 2006, p. 450.

[8] T.A. Haug, *Dissolution and Carbonation of Mechanically Activated Olivine* [Dissertation], Norwegian University of Science and Technology, Trondheim, 2010, p. 243.

[9] P. Baláž, *Mechanochemistry in Nanoscience and Minerals Engineering*, Springer, Verlag Berlin Heidelberg, 2008, p. 413.

[10] P. Pourghahramani, *Mechanical Activation of Hematite Using Different Grinding Methods with Special Focus on Structural Changes and Reactivity* [Dissertation], Luleå University of Technology, 2007. p. 117.

[11] K.L. Sandvik, R.A. Kleiv, and T.A. Haug, Mechanically activated minerals as a sink for CO_2, *Adv. Powder Technol.*, 22(2011), No. 3, p. 416.

[12] W.K. O'Connor, D.C. Dahlin, G.E. Rush, S.J. Gerdemann, L.R. Penner, and D.N. Nilsen, *Aqueous Mineral Carbonation*: *Mineral Availability*, *Pretreatment*, *Reaction Parametrics*, *and Process Studies*, Report No. DOE/ARC-TR-04-002, National Energy Technology Laboratory, Department of Energy, US, Albany, 2005, p. 462.

[13] P. Baláž, E. Turianicová, M. Fabián, R.A. Kleiv, J. Briančin, and A. Obut, Structural changes in olivine $(Mg, Fe)_2SiO_4$ mechanically activated in high-energy mills, *Int. J. Miner. Process*., 88(2008), No. 1-2, p. 1.

[14] C.A. Summers, D.C. Dahlin, G.E. Rush, W.K. O'Connor, and S.J. Gerdemann, Grinding methods to enhance the reactivity of olivine, [in] *SME Annual Meeting*, Denver, 2004, article number 04-93.

[15] D.J. Kim, J.S. Sohn, J.G. Ahn, and H.S. Chung, Extraction of Metals from Mechanically Milled Serpentine, *Geosyst. Eng.*, 11(2008), No. 2, p. 25.

[16] A. Drief and F. Nieto, The effect of dry grinding on antigorite from Mulhacen, Spain, *Clays Clay Miner.*, 47(1999), No. 4, p. 417.

[17] J. Yue and B. Klein, Particle breakage kinetics in horizontal stirred mills, *Miner. Eng.*, 18(2005), p. 325.

[18] B. Klein, J.S. Laskowski, and S.J. Partridge, A new viscometer for rheological measurements on settling suspensions, *J. Rheol.*, 39(1995), p. 827.

[19] A. Jankovic, Variables affecting the fine grinding of minerals using stirred mills, *Miner. Eng*., 16(2003), No. 4, p. 337.

[20] M.Z. He, Y.M. Wang, and E. Forssberg, Slurry rheology in wet ultrafine grinding of industrial minerals: a review, *Powder Technol.*, 147(2004), No. 1-3, p. 94.

[21] J. Yue and B. Klein, Influence of rheology on the performance of horizontal stirred mills, *Miner. Eng.*, 17(2004), No. 11-12, p. 1169.

[22] B.N. Ndlovu, E. Forbes, M. Becker, D.A. Deglon, J.P. Franzidis, and J.S. Laskowski, The effects of chrysotile mineralogical properties on the rheology of chrysotile suspensions, *Miner. Eng.*, 24(2011), No. 9, p. 1004.

[23] A.R. Reem, *The Effect of Stirred Mill Operation on Particles Breakage Mechanism and their Morphological Features* [Dissertation], University of British Columbia, Vancouver, 2011, p. 266.

[24] V.V. Boldyrev, S.V. Pavlov, and E.L. Goldberg, Interrelation between fine grinding and mechanical activation, *Int. J. Miner. Process.*, 44-45(1996), p. 181.

[25] C. Klein, C.S. Hurlbut, and J.D. Dana, *Manual of Mineralogy* (*21st Ed.*), John Wiley & Sons, New York, 1998, p. 532.

[26] S.M. Ohlberg and D.W. Strickler, Determination of percent crystallinity of partly devitrified glass by X-ray diffraction, *J. Am. Ceram. Soc.*, 45(1962), No. 4, p. 170.

[27] A.F. Gualtieri, C. Giacobbe, and C. Viti, The dehydroxylation of serpentine group minerals, *Am. Mineral*., 97(2012), p. 666.

[28] J. Hövelmann, H. Austrheim, A. Beinlich, and I.A. Munz, Experimental study of the carbonation of partially serpentinized and weathered peridotites, *Geochim. Cosmochim. Acta*, 75(2011), No. 22, p. 6760.

[29] K. Tkáčová and P. Baláž, Structural and temperature sensitivity of leaching of chalcopyrite with iron (III) sulphate, *Hydrometallurgy*, 21(1988), No. 1, p. 103.

[30] R. Lafay, G. Montes-Hernandez, E. Janots, R. Chiriac, N. Findling, and F. Toche, Simultaneous precipitation of magnesite and lizardite from hydrothermal alteration of olivine under high-carbonate alkalinity, *Chem. Geol.*, 368(2014), p. 63.

[31] S.J. Gerdemann, W.K. O'Connor, D.C. Dahlin, L.R. Penner, and H. Rush, *Ex situ* aqueous mineral carbonation, *Environ. Sci. Technol*., 41(2007), No. 7, p. 2587.